HHS Public Access

Author manuscript

*J Cardiovasc Electrophysiol*. Author manuscript; available in PMC 2015 April 16.

Published in final edited form as:

*J Cardiovasc Electrophysiol*. 2014 December ; 25(12): 1275–1283. doi:10.1111/jce.12514.

# Feasibility of Near Real-Time Lesion Assessment During Radiofrequency Catheter Ablation in Humans Using Acoustic Radiation Force Impulse Imaging

**Tristram D. Bahnson, M.D.**[*,†], **Stephanie A. Eyerly, Ph.D.**[‡], **Peter J. Hollender, Ph.D.**[‡], **Joshua R. Doherty, Ph.D.**[‡], **Young-Joong Kim, B.S.**[‡], **Gregg E. Trahey, Ph.D.**[‡,§], and **Patrick D. Wolf, Ph.D.**[‡]

[*]Duke Center for Atrial Fibrillation, Duke University Medical Center, North Carolina, USA

[†]Division of Cardiovascular Medicine, Cardiac Electrophysiology Section, Duke University Medical Center, North Carolina, USA

[‡]Department of Biomedical Engineering, Duke University Medical Center, North Carolina, USA

[§]Department of Radiology, Duke University Medical Center, North Carolina, USA

## Abstract

**Background—**Visual confirmation of radiofrequency ablation (RFA) lesions during clinical cardiac ablation procedures could improve procedure efficacy, safety, and efficiency. It was previously shown that acoustic radiation force impulse (ARFI) imaging can identify RFA lesions *in vitro* and *in vivo* in an animal model. This is the "first-in-human" feasibility demonstration of intracardiac ARFI imaging of RFA lesions in patients undergoing catheter ablation for atrial flutter (AFL) or atrial fibrillation (AF).

**Methods and Results—**Patients scheduled for right atrial (RA) ablation for AFL or left atrial (LA) ablation for drug refractory AF were eligible for imaging. Diastole-gated intracardiac ARFI images were acquired using one of two equipment configurations: (1) a Siemens ACUSON S2000™ ultrasound scanner and 8/10Fr AcuNav™ ultrasound catheter, or (2) a CARTO 3™ integrated Siemens SC2000™ and 10Fr SoundStar™ ultrasound catheter. A total of 11 patients (AFL = 3; AF = 8) were imaged. ARFI images were acquired of ablation target regions, including the RA cavotricuspid isthmus (CTI), and the LA roof, pulmonary vein ostia, posterior wall, posterior mitral valve annulus, and the ridge between the pulmonary vein and LA appendage. ARFI images revealed increased relative myocardial stiffness at ablation catheter contact sites after RFA and at anatomical mapping-tagged RFA treatment sites.

**Conclusions—**ARFI images from a pilot group of patients undergoing catheter ablation for AFL and AF demonstrate the ability of this technique to identify intra-procedure RFA lesion

Address for correspondence: Patrick Wolf, Ph.D., Department of Biomedical Engineering, Duke University, 136 Hudson Hall, P.O. Box 90281, Durham, NC 27708. Fax: 919-684-4488; patrick.wolf@duke.edu.

This manuscript was processed by a guest editor.

Biosense Webster and Siemens provided equipment for this study.

G.E. Trahey owns several patents in this area. Other authors: No disclosures.

formation. The results encourage further refinement of ARFI imaging clinical tools and continued investigation in larger clinical trials.

**Keywords**

acoustic radiation force impulse imaging; atrial fibrillation; atrial flutter; electroanatomical mapping; intracardiac echocardiography; lesion assessment; transcatheter radiofrequency ablation

## Introduction

Catheter ablation is used in contemporary clinical medicine to treat symptomatic cardiac tachyarrhythmias. Clinical efficacy of catheter-based radiofrequency ablation (RFA) for atrial fibrillation (AF) and atrial flutter (AFL) is dependent on successful creation of contiguous and transmural ablation lesions that produce targeted conduction block.[1,2] Whereas procedural efficacy with RFA requires delivery of ablative energy sufficient to produce such lesions, excess energy delivery can lead to complications such as cardiac perforation from “steam pops,” or injury to extra-cardiac structures such as the phrenic nerve, esophagus, pericardium, and lung.[3] Accordingly, methods to assess intra-procedural RFA lesion formation could improve procedure efficacy, safety, and efficiency.

To date, energy titration during RFA is largely empiric, relying on measurable variables such as ablation time, catheter tip temperature, power (watts), and ablation system impedance. However, these variables do not consistently predict lesion formation or size, and the gold standard for lesion assessment remains indirect via demonstration of conduction block and/or arrhythmia noninducibility.[4-7] Measurement of the contact-force between the catheter tip and the endocardial tissue is under investigation as an additional parametric predictor of RFA lesion formation, but cannot confirm actual lesion formation.[8-10] Despite a clinical demand, there is no widely available intra-procedural imaging method to directly assess RFA lesions *in vivo.*

Acoustic radiation force impulse (ARFI) imaging is an ultrasound-based method that creates high spatial resolution 2-dimensional (2-D) images of tissue elasticity.[11-15] ARFI imaging uses ultrasonic radiation force impulses to mechanically displace tissue, and conventional ultrasound methods to monitor the tissue response. The axial tissue displacement magnitude ($\sim$10 $\mu$m) is calculated using correlation based time-delay or phase-shift estimator methods.[16,17] The magnitude of the measured tissue displacement is inversely proportional to the tissue stiffness; in other words, stiffer tissue is displaced less than softer tissue when an equivalent acoustic radiation force is applied. Therefore, spatial variation within a 2-D image of ARFI-induced tissue displacement can identify relative differences in local tissue elasticity.[12,18,19]

RFA induced tissue heating causes irreversible thermocoagulation of intracellular and contractile proteins, which in turn reduces tissue viscoelasticity.[20,21] Although RFA does not produce long lasting detectable tissue changes in standard 2-D ultrasound images, it has been previously shown that ARFI imaging identifies discrete stiff regions that coincide with pathological RFA lesions both *in vitro*, and when imaging during diastole *in vivo* using animal models.[14,15,22-25] Further, in several of these *in vivo* studies, ARFI imaging was

implemented using conventional intracardiac echocardiography (ICE) imaging catheters and clinically available cardiac ablation mapping systems, and regions with “gaps” in the ablation line as identified with ARFI imaging were correlated with intact conduction.[15]

Intracardiac elastography methods such as ARFI imaging have never before been implemented in human patients and it remains unknown whether these techniques can be translated to humans. The large size of human atria compared with the animal model and the likelihood that there is a spectrum of tissue characteristics including fibrosis in human atria of some arrhythmia-prone individuals could well prevent successful ARFI imaging. Answers to these questions are prerequisites for further development of ARFI imaging tools or further studies to define the value of ARFI imaging with regard to procedure outcomes.

This report presents “first-in-man” ARFI images obtained during routine RFA for AF and AFL. The feasibility of ARFI imaging to identify ablated heart tissue in humans with paroxysmal or persistent AF and AFL and a spectrum of atrial morphologies is demonstrated using conventional and commercially available ultrasound catheters and ultrasound scanners.

## Methods

### Clinical Ablation Procedure

This study was approved by the institution review board at Duke University Medical Center Institutional on November 2, 2011, and subjects were imaged between June, 2012 and July, 2013. Individuals with planned right atrial (RA) ablation for AFL or left atrial (LA) ablation for symptomatic drug refractory AF were eligible, and all subjects granted informed consent. All patients received trans-thoracic echocardiograms within 3 months before their procedures, including routine measurement of the LA diameter.

In patients undergoing ablation for AFL, the ICE imaging and ablation catheters were positioned in the RA. For patients receiving treatment for AF, transseptal access was achieved under fluoroscopic and 2-D ICE guidance from the RA using routine techniques. Activated clotting times were maintained between 350 and 400 seconds using intravenous heparin, and the long sheaths were flushed with heparinized saline every 10–20 minutes while they were positioned in the LA. After transseptal access was obtained, the ICE imaging catheter was advanced to the LA through an 8.5Fr long sheath (8Fr AcuNav™; Siemens Healthcare, Issaquah, WA, USA), or directly across the transseptal puncture (10Fr AcuNav™/SoundStar™; Biosense Webster, Diamond Bar, CA, USA) and remained in the LA for the duration of LA mapping and ablation to provide direct visualization of ablation catheter-tissue contact quality and location during most RF-delivery, as is the standard of care for the primary operator. Standard continuous ICE images were available to the clinical operator at all portions of the procedure except when ARFI images were actively being acquired. ARFI images were obtained from 2 to 5 discrete locations in each subject at the operator's discretion. Positioning of the ICE catheter to obtain ARFI images was guided by biplane fluoroscopy, ICE, and when available, by the SoundStar projection of the ICE imaging plane on the CARTO3 (CartoSound, Biosense Webster, Diamond Bar, CA) electroanatomical mapping system (EAM). When acquiring an ARFI image, the ultrasound

transducer tip was positioned 1.5–2.5 cm from the endocardial site of interest, as indicated by the ICE distance scale. The catheter tip was oriented as parallel as possible to the endocardium and not more than 50° from the plane of the endocardial surface. These restrictions on ICE catheter-to-tissue orientation were selected to minimize depth-dependent energy attenuation, and to provide spatially consistent excitation across the field of view.

The AFRI imaging plane was directed to sites of ablation using one of two methods. For subjects imaged without the benefit of CartoSound imaging, the ablation catheter was placed against the endocardial surface of the RFA target. The ICE imaging plane was manipulated to clearly show the catheter tip, and once stability of the ICE imaging plane was confirmed, the ablation catheter was moved slightly out of the field of view, and baseline images were obtained. The ablation catheter was then returned to the imaging field and the lesion(s) were delivered; after RFA, the ablation catheter was again removed from the field of view so postablation ARFI images could be obtained. This entire process took 2–5 minutes (see Fig. 3). For subjects imaged with the SoundStar catheter, the ICE imaging plane projected by the EAM system was guided to previously annotated ablation sites for ARFI imaging.

The goal of this study was to determine whether ARFI imaging could be adapted to the clinical electrophysiology laboratory, identify RFA lesions *in vivo*, and obtain images from endocardial regions relevant for therapeutic ablation. With this in mind, the additional procedure time allowed to obtain ARFI images was restricted to ≤ 15 minutes per subject so as not to significantly prolong the procedure, to minimize risk to patients, and confirm that interpretable images could be acquired within a reasonable time. Accordingly, only 2–5 images were obtained per patient. The ARFI image data were not used to alter treatment; specifically, the operator was blinded to the processed ARFI images, and ARFI image data were not used to guide RFA lesion delivery.

### ARFI Imaging Implementation

Two imaging platforms were used: (1) a custom ARFI imaging tool developed for the S2000™ (Siemens Healthcare) ultrasound scanner and the 8Fr or 10Fr AcuNav, and (2) an externally driven (laptop) ARFI imaging software for the SC2000™ (Siemens Healthcare) and integrated with the CARTO3 and 10Fr SoundStar (Biosense Webster). Images generated using the S2000 system displayed ARFI displacement information on the 2-D ICE image whereas ARFI images from the SC2000 were displayed against a black background. Each software platform allowed rapid acquisition of co-registered ICE and ARFI images during the clinical procedure. The imaging platforms also transitioned quickly between live ICE and ARFI imaging modes as needed for the clinical procedure. Of note is that the ARFI and ICE imaging planes are one in the same, and for CartoSound cases the ICE imaging plane registration to the EAM and tagged ablation points was inherent to the imaging system, and was independent of operator input or adjustment.

The ARFI imaging sequences underwent safety testing to confirm the measured mechanical index (MI) and transducer surface temperature rise (dT) were within the FDA limits (MI < 1.8, FDA limit 1.9; single ARFI image acquisition dT∼0.8 °C in standing water, ICE dT∼2.6 °C, FDA limit 6.0 °C).[26] The S2000 platform acquired ARFI images with a transmit and tracking frequency of 6.15 MHz and a tracking pulse repetition frequency (PRF) of 9

kHz. Each ARFI line was acquired with parallel receive tracking (2:1) for 0.6–1.5 ms post-ARFI excitation. The SC2000-CARTO3 platform acquired ARFI images with a frequency of 6 MHz and a PRF of 16 kHz. Each ARFI line was acquired with parallel receive tracking (8:1) for 2.5 ms post-ARFI excitation. Completion of each 2-D image acquisition took less than 100 ms, and the ARFI image lateral field of view was 30–45° (traditional ICE provides 90°). An ARFI imaging focal depth 1.0–2.25 cm was operator selected at each imaging location to position the imaging focus within the myocardium.

It has been shown that diastolic imaging is ideal to resolve lesions *in vivo* because the contrast between the stiff RFA lesion and normal tissue decreases during myocardial contraction, and late diastole is the time of least intrinsic motion during the cardiac cycle.[13,15] The diastolic imaging period was operator selected. Therefore, all ARFI images acquired in this pilot study were ECG-gated to atrial diastole during normal sinus rhythm (NSR) or during atrial pacing. It was not possible to obtain baseline images before RF-energy delivery commenced in patients who were initially in AF or AFL; in these individuals, ARFI images were obtained of ablation target sites after NSR had been restored.

### ARFI Image Processing

Preliminary ARFI images were available within 5 seconds to confirm successful image acquisition; raw data were saved and re-processed later for final images. ARFI imaging was not dependent on the availability of baseline images because the technique displays relative tissue displacement pixel to pixel across the imaging field. The measured ARFI-induced displacements were calculated using a phase-shift algorithm (Loupas, axial kernel = 1.5λ).[17] Poor displacement estimates were removed from the image by thresholding the magnitude of the correlation coefficient of the phase-shift estimation.[17] The measured displacement temporal profiles were filtered to separate ARFI-induced motion from bulk cardiac and respiratory motion, and the maximum ARFI-induced displacement through the tracking time was found at each pixel location.[15,22,27] Patient motion did not interfere with imaging in these patients with general anesthesia or deep conscious sedation. The 2-D pixel data was spatially filtered (25×5 pixel median filter in S2000 images, 6×6 pixel averaging filter in SC2000 images). The final color display is the maximum ARFI-induced displacement (microns) at each pixel, and the color scale was adjusted in each image to span the observed displacements to best resolve relative differences in tissue elasticity within the imaged field of view.

## Results

Eleven subjects (59 ± 8 years of age, 1 woman) had imaging attempted during their ablation procedures. Two subjects were imaged in the RA during ablation of the cavotricuspid isthmus (CTI) for typical AFL, and the remainder received LA imaging during ablation for AF (n = 8) or atypical AFL (n = 1). Interpretable images showing tissue stiffening consistent with RFA lesions where RFA pulses had been delivered were obtained from 1-4 sites in all but one of the subjects. The subject for whom images could not be obtained received ablation at the LA roof for atypical AFL. Images were not obtained because the subject remained in AFL for the majority of the study preventing diastolic gating, and the tip of the

ICE catheter could not be manipulated to within 2.5 cm of the LA roof. Five patients began the procedure in normal rhythm, and image data from these patients pre- and post-ablation are depicted in Figures 1, 3, and 4. The remainder of patients were imaged after NSR had been restored; the lack of baseline imaging in these subjects did not prevent recognition of focal increased tissue stiffness at tagged sites of prior ablation, and no subjects demonstrated focal regions of increased stiffness when imaging unablated regions.

The arrhythmia pattern and atrial sizes were variable across subjects, demonstrating that ARFI imaging is possible in individuals with a spectrum of atria morphology. Atrial sizes ranged from 3.6 to 5.2 cm (4.4 ± 0.5 cm; mean ± SD). A summary of the patient procedures, arrhythmia types, and the imaging platforms is presented in Table 1.

No subject had peri-procedural (±7 days) stroke, retroperitoneal bleeding, groin hematoma, cardiac perforation, cardiac tamponade, or a pericardial effusion.

### Right Atrial Imaging Results

Figure 1 shows images before and after RFA lesion delivery at the CTI. Figure 2 shows an ARFI image after an initial 40–60s RF-pulse at the tendon of Todaro. The tissue proximate to the valve was stiffer than adjacent tissue consistent with an RFA lesion; “soft” or compliant tissue remained on the inferior vena cava (IVC) ostia side of the ligament consistent with incomplete CTI ablation. Based on independent clinical criteria, additional ablation adjacent to the IVC ostium was delivered before CTI block was achieved in this subject. These images demonstrate that regions relevant to RA ablation of typical AFL can be ARFI imaged, and tissue changes consistent with RFA lesion formation can be resolved.

### Left Atrium Imaging Results

ARFI imaging of the posterior LA wall immediately following an RF-pulse (35W, 60s) was accomplished and demonstrated discrete tissue changes from the baseline image at the RFA site consistent with successful imaging of this region (data not shown). Further, three sequential images at this site, obtained over 20 seconds, showed reproducible identification of the tissue elasticity changes at the RFA site.

Figure 3 depicts ARFI imaging of RFA sites at the LA roof. Tissue stiffening, relative to adjacent unablated tissue in the field of view, is produced by the sequential application of RF energy. The initial ablation near the left of each panel produced tissue stiffening that was reproducibly imaged over a period of the several minutes. ICE and ARFI images were obtained of the superior portion of the ligament of Marshall (LoM) at the ridge between the left atrial appendage (LAA) and left pulmonary veins (LPVs) in several patients. Figure 4 shows ARFI images of the LoM from a representative patient before and after two RF-pulses. ARFI images revealed limited increased stiffness (decreased tissue displacement) consistent with nontransmural RFA lesions at the RF-delivery sites, suggesting that complete ablation of the LoM had not been achieved after the initial RF-pulses.

ARFI imaging was successfully integrated with the CARTO3-SoundStar system as depicted in Figures 5 and 6. The EAM mapping system allowed the imaging plane to be directed to sites of previous ablation at any time during the procedure. Figures 5 and 6 also show tissue

changes at sites of prior RFA that are recognized during re-imaging 15–75 minutes after initial ablation. Accordingly, ARFI imaging identifies changes after ablation that are long lasting, and yields reproducible images of discrete tissue changes coincident with the sites of RF energy delivery.

Further, ARFI identified a discrete region consistent with incomplete ablation that corresponded with the region of conduction breakthrough at the right inferior PV (Fig. 5) suggesting potential for evaluation of previously delivered lesion sets. The posterior mitral annulus (MA) was also imaged (Fig. 6) and tissue changes consistent with RFA lesions identified.

## Discussion

This is the first demonstration of intracardiac ARFI imaging of atrial myocardium in human patients with AFL and AF. ARFI images visualized discrete changes in relative tissue stiffness coincident with RFA lesion delivery and consistent with near real-time confirmation of RFA lesion formation. In aggregate, Figures 1 through 6 demonstrate that tissue stiffness changes are consistently observed in regions that had been targeted with RFA. Further, successful images were collected at the RA CTI including the tendon of Todaro, and at the LA roof, the posterior LA wall, the LoM, the right PV antra, and the posterior LA adjacent to the coronary sinus; these regions are important targets during catheter ablation for AFL and AF.

Both intracardiac ultrasound and electroanatomic mapping are widely used to guide transseptal catheterization and monitor the location of RFA delivery. This study suggests that implementation of ARFI imaging during routine clinical care could be accomplished should clinical utility be confirmed with future prospective studies, and should optimized imaging tools become available.

Demonstration of feasibility of intracardiac ARFI imaging as a valid elastography method for imaging in humans is a prerequisite for studies that define the utility of these techniques to visualize acute and/or chronic lesions. In addition, these methods for near real-time lesion assessment could also be a powerful tool to assess lesion formation with new ablation technologies, and to better define the relationships between lesion size and ablation parameters such as power, tip temperature, ablation duration, and catheter contact-force. The ability to do intra-procedural lesion assessment could also improve safety by confirming the minimum RF-energy required to achieve lesion transmurality and allowing avoidance of excessive RF-energy delivery. Finally, this technology could be further developed to allow tissue characterization based upon regional tissue compliance or the variation in tissue compliance between regions of the heart in the individual.

It is possible that lesion formation is also influenced by tissue characteristics including fibrosis and local LA anatomy; for example, although anecdotal, Figure 4 shows that a 60s RF-pulse with ICE-confirmed catheter-tip tissue contact did not appear to produce complete transmural lesions at the LoM. This is consistent with prior reports that PV reconnection is frequently observed at this location,[28] perhaps related to difficulty in achieving adequate

contact-force.[9,10] Also, it has been reported that gaps in an ablation line may not always be distinguishable using acute conduction block criteria.[7] ARFI imaging could improve the efficacy of ablation especially in "difficult to ablate" regions where lesion completeness and durability are hard to assess.

To date, MRI is the best currently available clinical tool for assessing tissue fibrosis and visualizing ablation lesion patterns.[29-32] While promising as a pre- and post-procedure substrate and lesion assessment tool, MRI has limitations for intra-procedural imaging due to the necessity for nonmetallic catheters and lengthy image acquisition times. Also, recent studies have concluded that current methods of MRI assessment of atrial RFA lesions show limited resolution for characterizing small gaps in an ablation line.[33,34] Intracardiac ARFI imaging provides higher spatial resolution (sub-millimeter) than current MRI methods.[25]

An ongoing question regarding *in vivo* ARFI imaging after RFA is whether transient tissue edema could mimic elasticity changes produced by coagulation necrosis. Of note is that in previous studies gross-pathologically identified RFA lesions were consistent in size and morphology to ARFI imaging lesion assessments in an *ex vivo* muscle prep incapable of becoming edematous, and *in vivo* using an animal model.[15,23-25]Additional unpublished data suggest that ARFI-identified RF lesions in an animal model are of constant size during the 30 minute peri-ablation period. While these observations do not exclude that tissue edema contributes to the observed tissue elasticity changes, it seems likely that coagulation necrosis is also a significant contributor.

## Considerations for Widespread Clinical Translation

The standout challenge encountered during this initial experience using intra-procedural ARFI imaging was to position the ICE imaging catheter relatively parallel to and within 2.5 cm of all regions of interest in all patients. Quick and efficient maneuvering of the imaging catheter to within 2.5 cm of the chamber wall was at times difficult, especially in patients with large atria, or those for whom an imaging target was far from the path of the imaging catheter tip as it was advanced in the LA. To prepare this technology for future trials and widespread clinical adoption, it is estimated that an ARFI imaging range of 4–6 cm would be ideal. This range would improve the likelihood of consistently imaging regions of interest. The solution to this obstacle will likely require the development of optimized systems for ARFI imaging that include improvements in catheter steering mechanisms, improved steerable sheaths, or modifications to the ultrasound transducer. The catheter manipulation techniques needed to obtain useful images are routinely practiced at our institution; additional training to implement ARFI imaging would be minimal for current experienced clinical operators given that the system uses many components of existing and familiar clinical imaging tools.

Existing electroanatomic map integrated ICE imaging greatly facilitated the ability to direct ARFI imaging to RFA sites during the procedure. As implemented, the guidance system was essential to efficiently positioning the ARFI imaging plane over RFA lesions; it is not recommended that ARFI imaging evaluations of lesions be implemented without this guidance until ARFI can provide rapid acquisition 3-D ARFI images with an extended field of view.

It is possible to acquire ARFI images during AF; but while the images can be ECG-gated to ventricular diastole to help reduce motion artifacts, the atrial tissue stiffening associated with AF is random, and can prevent recognition of the discrete and focal elasticity changes produced by RFA lesions. In these clinical patients, the heart was frequently in AF during the beginning of the procedure, and ARFI images during AF exhibited substantial motion artifacts that yielded inconclusive images. While imaging during AFL or AF was beyond the scope of this feasibility demonstration, effective methods for imaging lesions during AFL or AF are being investigated and would provide more imaging opportunities during the preablation portion of the procedure.

### Study Limitations

This paper demonstrates that ARFI imaging can resolve changes in myocardial tissue stiffness coincident with RF ablation. Based upon knowledge of the mechanisms of RFA lesion formation and animal studies of ARFI that include histologic analysis, it is very likely that the observed tissue changes described here represent RFA lesion formation. However, one cannot yet conclude with certainty that the appearance of transmural and contiguous regions of tissue stiffening are equivalent to the formation of durable RFA lesions that result in long-term conduction block. Whereas animal studies found clear correlation between demonstrable conduction block and ARFI images, further prospective studies are required to demonstrate that a complete transmural and contiguous lesion set in ARFI images corresponds with durable conduction block or procedural outcome in humans.[15]

Nonetheless, the body of *in vitro* and *in vivo* animal data together with the demonstrated feasibility of imaging important clinical RFA targets in humans is noteworthy and recommends further investigation.

## Conclusions

This study demonstrated the clinical feasibility of intra-procedure ARFI imaging in humans with a spectrum of atrial morphology. ARFI imaging identified tissue changes resulting from RFA consistent with near real-time recognition of lesion formation with high spatial resolution. The technique can be applied to image RA and LA regions important for therapeutic catheter ablation. This imaging technique can be adapted to widely available ICE catheters, ultrasound consoles, and electroanatomic mapping systems although further development of imaging tools would enhance clinical utility. The ultrasound energy delivered in order to obtain ARFI images is below the FDA limits for ICE imaging. Further studies are warranted to define how tissue characteristics affect ARFI imaging, to optimize the imaging technique for use during clinical care, and to explore the relationship between ARFI identified tissue changes and procedure outcome.

## Acknowledgments

This study used loaned equipment from Siemens Healthcare (ACUSON S2000™ and SC2000™ ultrasound scanners: Issaquah, WA, USA) and Biosense Webster (CARTO3™ with CartoSound™: Diamond Bar, CA). We would like to thank Douglas Dumont and Stephen Rosenzweig for their help with the scanner software development, Steve Guerrant for his technical and equipment assistance in the clinic, as well as the staff in the Duke University Medical Center EP labs for their patience and support during the procedures.

Funding for this study was provided by NIH grant numbers R01-EB-012484, R21-EB-007741, and R37-HL-096023.

## References

1. Cappato R, Calkins H, Chen SA, Davies W, Iesaka Y, Kalman J, Kim YH, Klein G, Natale A, Packer D, Skanes A, Ambrogi F, Biganzoli E. Updated worldwide survey on the methods, efficacy, and safety of catheter ablation for human atrial fibrillation. Circ Arrhythm Electrophysiol. 2010; 3:32–38. [PubMed: 19995881]
2. Eckstein J, Zeemering S, Linz D, Maesen B, Verheule S, van Hunnik A, Crijns H, Allessie MA, Schotten U. Transmural conduction is the predominant mechanism of breakthrough during atrial fibrillation: Evidence from simultaneous endo-epicardial high-density activation mapping. Circ Arrhythm Electrophysiol. 2013; 6:334–341. [PubMed: 23512204]
3. Deshmukh A, Patel NJ, Pant S, Shah N, Chothani A, Mehta K, Grover P, Singh V, Vallurupalli S, Savani GT, Badheka A, Tuliani T, Dabhadkar K, Dibu G, Reddy YM, Sewani A, Kowalski M, Mitrani R, Paydak H, Viles-Gonzalez JF. In-hospital complications associated with catheter ablation of atrial fibrillation in the United States between 2000 and 2010: Analysis of 93 801 procedures. Circulation. 2013; 128:2104–2112. [PubMed: 24061087]
4. Calkins H, Kuck KH, Cappato R, Brugada J, Camm AJ, Chen SA, Crijns HJ, Damiano RJ Jr, Davies DW, DiMarco J, Edgerton J, Ellenbogen K, Ezekowitz MD, Haines DE, Haissaguerre M, Hindricks G, Iesaka Y, Jackman W, Jalife J, Jais P, Kalman J, Keane D, Kim YH, Kirchhof P, Klein G, Kottkamp H, Kumagai K, Lindsay BD, Mansour M, Marchlinski FE, McCarthy PM, Mont JL, Morady F, Nademanee K, Nakagawa H, Natale A, Nattel S, Packer DL, Pappone C, Prystowsky E, Raviele A, Reddy V, Ruskin JN, Shemin RJ, Tsao HM, Wilber D. Heart Rhythm Society Task Force on Catheter and Surgical Ablation of Atrial Fibrillation. 2012 HRS/EHRA/ECAS expert consensus statement on catheter and surgical ablation of atrial fibrillation: Recommendations for patient selection, procedural techniques, patient management and follow-up, definitions, endpoints, and research trial design. Heart Rhythm. 2012; 9:632–696 e621. [PubMed: 22386883]
5. Haines DE. The yin and yang of convective cooling in radiofrequency catheter ablation. Circ Arrhythm Electrophysiol. 2011; 4:794–795. [PubMed: 22203658]
6. Sy RW, Thiagalingam A, Stiles MK. Modern electrophysiology mapping techniques. Heart Lung Circ. 2012; 21:364–375. [PubMed: 22575530]
7. Miller MA, d'Avila A, Dukkipati SR, Koruth JS, Viles-Gonzalez J, Napolitano C, Eggert C, Fischer A, Gomes JA, Reddy VY. Acute electrical isolation is a necessary but insufficient endpoint for achieving durable PV isolation: The importance of closing the visual gap. Europace. 2012; 14:653–660. [PubMed: 22417723]
8. Martinek M, Lemes C, Sigmund E, Derndorfer M, Aichinger J, Winter S, Nesser HJ, Purerfellner H. Clinical impact of an open-irrigated radiofrequency catheter with direct force measurement on atrial fibrillation ablation. Pacing Clin Electrophysiol. 2012; 35:1312–1318. [PubMed: 22946636]
9. Reddy VY, Shah D, Kautzner J, Schmidt B, Saoudi N, Herrera C, Jais P, Hindricks G, Peichl P, Yulzari A, Lambert H, Neuzil P, Natale A, Kuck KH. The relationship between contact force and clinical outcome during radiofrequency catheter ablation of atrial fibrillation in the TOCCATA study. Heart Rhythm. 2012; 9:1789–1795. [PubMed: 22820056]
10. Neuzil P, Reddy VY, Kautzner J, Petru J, Wichterle D, Shah D, Lambert H, Yulzari A, Wissner E, Kuck KH. Electrical reconnection after pulmonary vein isolation is contingent on contact force during initial treatment: Results from the EFFICAS I study. Circ Arrhythm Electrophysiol. 2013; 6:327–333. [PubMed: 23515263]
11. Doherty JR, Trahey GE, Nightingale KR, Palmeri ML. Acoustic radiation force elasticity imaging in diagnostic ultrasound. IEEE Trans Ultrason Ferroelectr Freq Control. 2013; 60:685–701. [PubMed: 23549529]
12. Nightingale K, Palmeri M, Frinkley K, Sharma A, Zhai L, Trahey G. Ultrasonic imaging of the mechanical properties of tissues using localized, transient acoustic radiation force. Int Conf Acoust Spee. 2005; 5:981–984.
13. Hsu, SJ. Biomedical Engineering PhD Dissertation. Duke University; 2009. Acoustic Radiation Force Impulse Imaging of Myocardial Stiffness.

14. Fahey BJ, Nightingale KR, McAleavey SA, Palmeri ML, Wolf PD, Trahey GE. Acoustic radiation force impulse imaging of myocardial radiofrequency ablation: Initial in vivo results. IEEE Trans Ultrason Ferroelectr Freq Control. 2005; 52:631–641. [PubMed: 16060512]
15. Eyerly SA, Bahnson TD, Koontz JI, Bradway DP, Dumont DM, Trahey GE, Wolf PD. Intracardiac acoustic radiation force impulse imaging: A novel imaging method for intraprocedural evaluation of radiofrequency ablation lesions. Heart Rhythm. 2012; 9:1855–1862. [PubMed: 22772134]
16. Pinton GF, Dahl JJ, Trahey GE. Rapid tracking of small displacements with ultrasound. IEEE Trans Ultrason Ferroelectr Freq Control. 2006; 53:1103–1117. [PubMed: 16846143]
17. Loupas T, Powers JT, Gill RW. An axial velocity estimator for ultrasound blood-flow imaging, based on a full evaluation of the doppler equation by means of a 2-dimensional autocorrelation approach. IEEE Trans Ultrason Ferroelectr Freq Control. 1995; 42:672–688.
18. Palmeri ML, Sharma AC, Bouchard RR, Nightingale RW, Nightingale KR. Afinite-element method model of soft tissue response to impulsive acoustic radiation force. IEEE Trans Ultrason Ferroelectr Freq Control. 2005; 52:1699–1712. [PubMed: 16382621]
19. Nightingale K, Palmeri M, Trahey G. Analysis of contrast in images generated with transient acoustic radiation force. Ultrasound Med Biol. 2006; 32:61–72. [PubMed: 16364798]
20. Pernot M, Mace E, Dubois R, Couade M, Fink M, Tanter M. Mapping myocardial elasticity changes after RF-ablation using supersonic shear imaging. Comput Cardiol. 2009; 2009:793–796.
21. Wright NT, Humphrey JD. Denaturation of collagen via heating: An irreversible rate process. Annu Rev Biomed Eng. 2002; 4:109–128. [PubMed: 12117753]
22. Hsu SJ, Fahey BJ, Dumont DM, Wolf PD, Trahey GE. Challenges and implementation of radiation-force imaging with an intracardiac ultrasound transducer. IEEE Trans Ultrason Ferroelectr Freq Control. 2007; 54:996–1009. [PubMed: 17523564]
23. Eyerly SA, Hsu SJ, Agashe SH, Trahey GE, Li Y, Wolf PD. An in vitro assessment of acoustic radiation force impulse imaging for visualizing cardiac radiofrequency ablation lesions. J Cardiovasc Electrophysiol. 2010; 21:557–563. [PubMed: 20021518]
24. Eyerly SA, Dumont DM, Trahey GE, Wolf PD. In vitro monitoring of the dynamic elasticity changes during radiofrequency ablation with acoustic radiation force impulse imaging. J Cardiovasc Electrophysiol. 2013; 24:472–473. [PubMed: 23140364]
25. Eyerly SA, Bahnson TD, Koontz JI, Bradway DP, Dumont DM, Trahey GE, Wolf PD. Contrast in intracardiac acoustic radiation force impulse images of radiofrequency ablation lesions. Ultrason Imaging. 2014; 36:133–148. [PubMed: 24554293]
26. Nelson TR, Fowlkes JB, Abramowicz JS, Church CC. Ultrasound biosafety considerations for the practicing sonographer and sonologist. J Ultrasound Med. 2009; 28:139–150. [PubMed: 19168764]
27. Giannnantonio DM, Dumont DM, Trahey GE, Byram BC. Comparison of physiological motion filters for cardiac ARFI. Ultrason Imaging. 2011; 33:89–108. [PubMed: 21710825]
28. Cappato R, Negroni S, Pecora D, Bentivegna S, Lupo PP, Carolei A, Esposito C, Furlanello F, De Ambroggi L. Prospective assessment of late conduction recurrence across radiofrequency lesions producing electrical disconnection at the pulmonary vein ostium in patients with atrial fibrillation. Circulation. 2003; 108:1599–1604. [PubMed: 12963643]
29. Akoum N, Daccarett M, McGann C, Segerson N, Vergara G, Kuppahally S, Badger T, Burgon N, Haslam T, Kholmovski E, Macleod R, Marrouche N. Atrial fibrosis helps select the appropriate patient and strategy in catheter ablation of atrial fibrillation: A DE-MRI guided approach. J Cardiovasc Electrophysiol. 2011; 22:16–22. [PubMed: 20807271]
30. Kolandaivelu A, Zviman MM, Castro V, Lardo AC, Berger RD, Halperin HR. Noninvasive assessment of tissue heating during cardiac radiofrequency ablation using MRI thermography. Circ Arrhythm Electrophysiol. 2010; 3:521–529. [PubMed: 20657028]
31. Vergara GR, Vijayakumar S, Kholmovski EG, Blauer JJE, Guttman MA, Gloschat C, Payne G, Vij K, Akoum NW, Daccarett M, McGann CJ, Macleod RS, Marrouche NF. Real-time magnetic resonance imaging-guided radiofrequency atrial ablation and visualization of lesion formation at 3 Tesla. Heart Rhythm. 2011; 8:295–303. [PubMed: 21034854]
32. Harrison JL, Jensen HK, Peel SA, Chiribiri A, Grondal AK, Bloch LO, Pedersen SF, Bentzon JF, Kolbitsch C, Karim R, Williams SE, Linton NW, Rhode KS, Gill J, Cooklin M, Rinaldi CA,

Wright M, Kim WY, Schaeffter T, Razavi RS, O'Neill MD. Cardiac magnetic resonance and electroanatomical mapping of acute and chronic atrial ablation injury: A histological validation study. Eur Heart J. 2014; 35:1486–1495. [PubMed: 24419806]

33. Hunter RJ, Jones DA, Boubertakh R, Malcolme-Lawes LC, Kanagaratnam P, Juli CF, Davies DW, Peters NS, Baker V, Earley MJ, Sporton S, Davies LC, Westwood M, Petersen SE, Schilling RJ. Diagnostic accuracy of cardiac magnetic resonance imaging in the detection and characterization of left atrial catheter ablation lesions: A multicenter experience. J Cardiovasc Electrophysiol. 2013; 24:396–403. [PubMed: 23293924]
34. Ranjan R, Kato R, Zviman MM, Dickfeld TM, Roguin A, Berger RD, Tomaselli GF, Halperin HR. Gaps in the ablation line as a potential cause of recovery from electrical isolation and their visualization using MRI. Circ Arrhythm Electrophysiol. 2011; 4:279–286. [PubMed: 21493875]

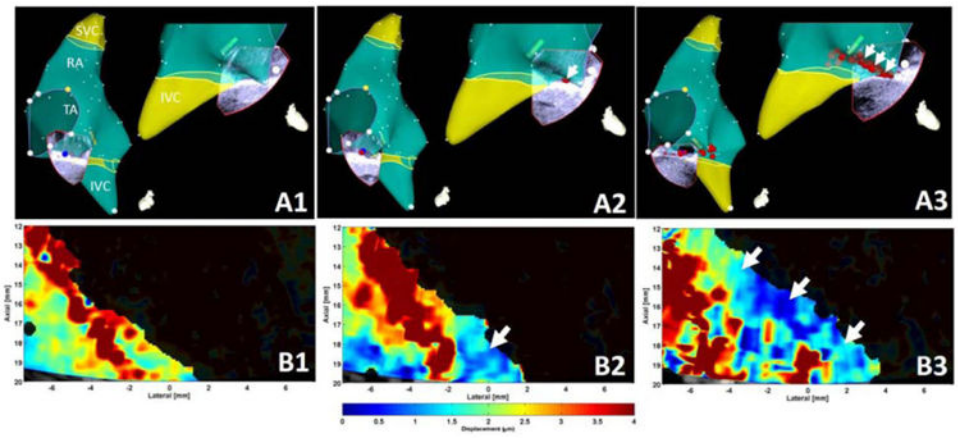


**Figure 1.**

CARTO3 maps and corresponding ARFI images from a patient undergoing ablation for typical AFL. Row A: ICE imaging planes are projected onto the CARTO3 maps. Row B: ARFI images obtained before (column 1), after a single 60s RF-pulse (column 2, red sphere), and after additional ablation along the cavotricuspid isthmus (CTI) (column 3). B2 shows a distinct decrease in the ARFI-induced tissue displacement (increased stiffness, blue end of color scale) at the focal ablation site near the tricuspid valve annulus (TA, arrow, imaged ∼4 min after RFA). After additional ablation along the CTI (B3, arrows), a contiguous region of increased stiffness became apparent. Bi-directional conduction block at the CTI was later confirmed.

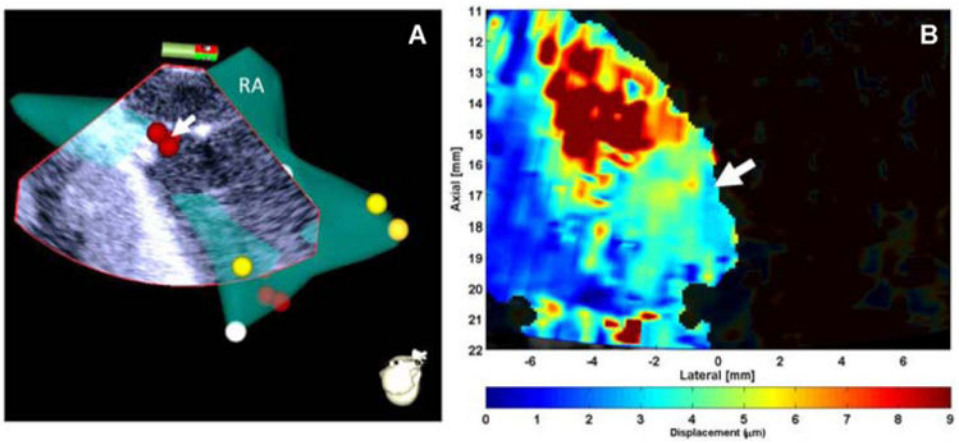


**Figure 2.**

CARTO3 map with the projected ICE imaging plane (panel A) and the corresponding ARFI image (panel B) in another patient undergoing CTI ablation for typical AFL. The ARFI image was obtained ∼20 min after three 45–60s RF-pulses were delivered (red tags) at the TA side of the tendon of Todaro. The TA region is in the lower right corner, and the inferior vena cava (IVC) ostia region is at the upper left corner of the image. ARFI imaging revealed that there is a local transmural increase in relative tissue stiffness at the site of RFA (arrow, panel B) compared with adjacent myocardium, consistent with incomplete ablation of this region. The ablation line was subsequently extended to the IVC ostium to produce conduction block across the CTI.

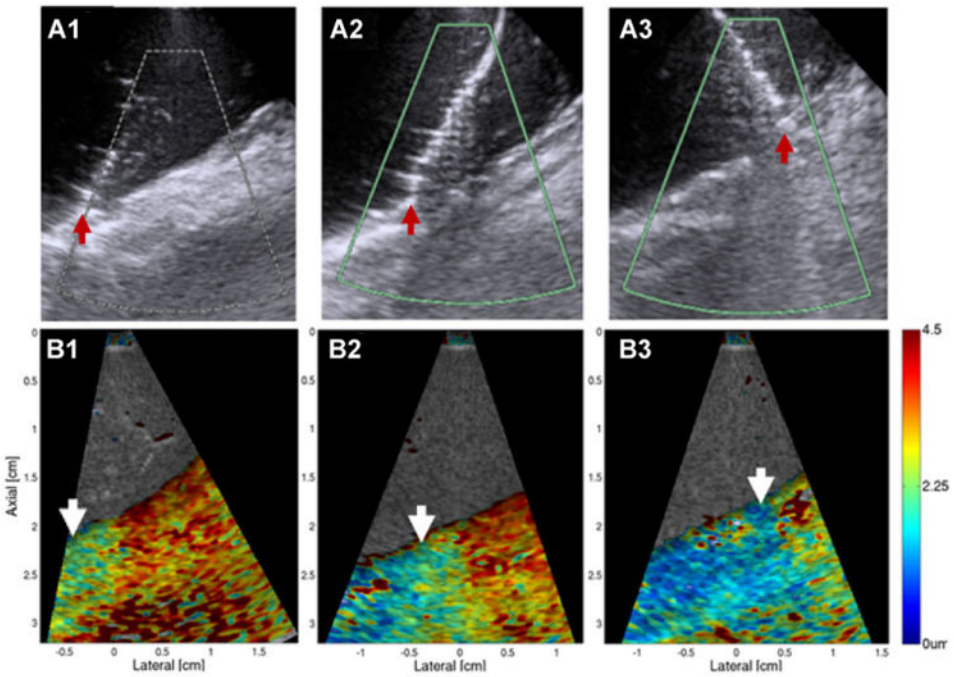


**Figure 3.**

ICE and ARFI images of ablation catheter contact locations (red arrows, row A) for three consecutive RF-pulses (irrigated, 35W power-controlled, 60s each) delivered at the LA roof. The corresponding ARFI images were obtained within 2 min of each RF-pulse at the ablation catheter contact location (row A). Panel B1 serves as a “baseline” image for panel B2, and panel B2 serves as a “baseline” image for panel B3. White arrows indicate the newly formed regions of increased tissue stiffness after RF-pulses. A distinct border between myocardium and pericardium is difficult to discern with the 2-D images and is most evident in panel A2. The tissue thickness appears to be approximately 5 mm; ARFI image pseudocoloring extends past this boundary consistent with transmural lesions. The position and orientation of the ICE catheter was maintained between acquisitions, but note that the ARFI imaging plane in B1 was steered (an operator capability included on the clinical software platform) slightly to the right compared to panels B2 and B3 to keep the ablation catheter out of the field of view during ARFI imaging of B1.

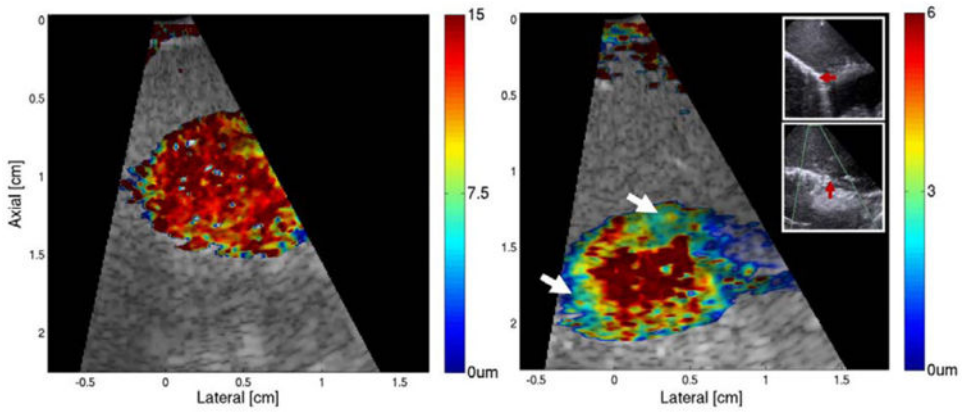


**Figure 4.**

ARFI image at the ligament of Marshall (LoM) before and after ablation. The insets show 2-D ICE images of the location of each of two RF-pulses delivered at the LoM in this subject immediately prior to ARFI imaging. RF-delivery locations are depicted by the red arrows (35W for 30s, top inset, and 35W for 60s, bottom inset). Resultant regions of reduced displacement (increased stiffness) on the ARFI images are indicated with the larger white arrows. In both panels, the left superior pulmonary vein (LSPV) lumen is at the bottom. No RF-energy had been delivered at these locations prior to delivery of the RF-pulses depicted in the insets. Note the absolute value of the ARFI-induced displacements were higher in the baseline image because the imaging catheter was positioned closer.

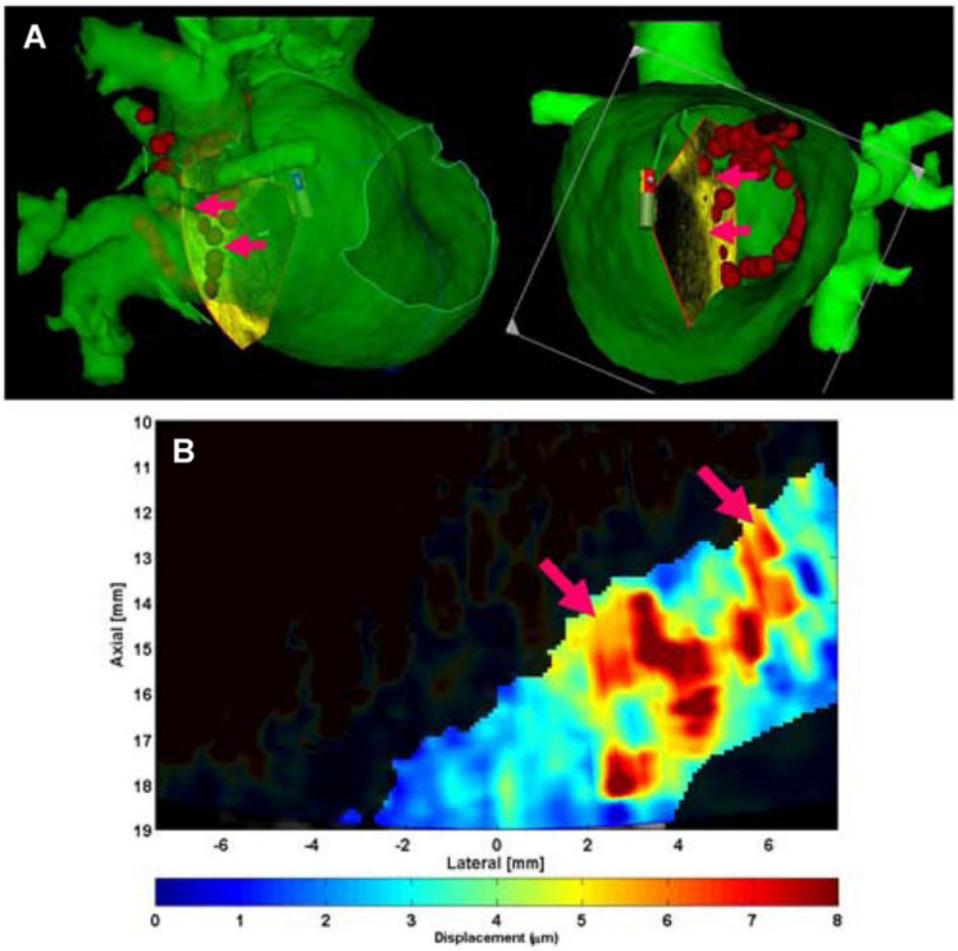


**Figure 5.**

CARTO3 map with a registered MRI image and ARFI image of the septal margin of the right inferior pulmonary vein (RIPV). Panel A depicts the segmented, merged, and registered MRI image that is partially transparent and displayed in the right anterior oblique, and left anterior oblique views (clipped view with left half of the LA removed). The locations of RFA energy delivery were marked with red spheres using the mapping system 30–60 min prior to ARFI image acquisition. Multiple RF lesions had been delivered around the right PVs. The ICE image plane is superimposed on the MRI with the orientation determined by the EAM system; visualization of the ICE imaging plane was available to the operator in real-time and was used to direct the imaging plane to overlap with tagged ablation sites to obtain the ARFI image in Panel B. Panel B depicts the ARFI image of a site near prior ablation where the magenta arrows highlight local regions of higher displacement soft tissue between regions of stiff tissue suggesting incomplete ablation. After ARFI imaging, interrogation of this vein with a circular mapping catheter revealed persistent PV connection that was localized to the septal aspect of the right inferior PV antrum near where ARFI imaging suggested incomplete ablation. RFA directed to this site, based on circular mapping catheter electrogram recordings, produced PV isolation.

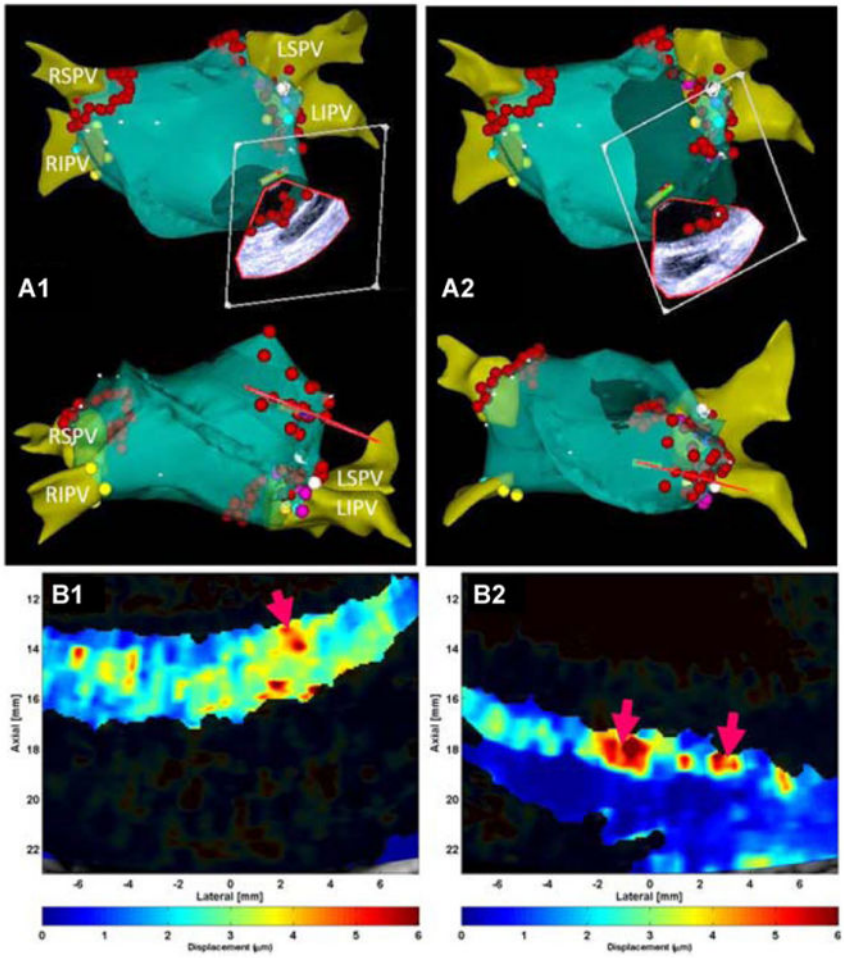


**Figure 6.**

CARTO3 map of the LA (A) and ARFI images (B) of the posterior MA. The 2-D ICE imaging plane is directed toward the MA adjacent to the coronary sinus. Multiple RF lesions had been delivered at the mitral annulus as depicted by the red tags on the EAM. Two slightly different imaging planes were obtained during interrogation of this region are shown in panels A1 and A2. As in Figure 5, the projected ICE imaging plane was visible to the operator in real-time and used to direct ARFI imaging to the region of prior ablation. The corresponding ARFI images are shown in panels B1 and B2. The ARFI images show nonhomogeneous tissue elasticity; the magenta arrows identify regions with compliant or soft tissue. Alteration of local tissue elasticity due to intracardiac catheters such as a coronary sinus catheter cannot be excluded; however, tissue stretch due to a catheter would not be expected to produce discrete focal regions of decreased elasticity within the imaging field.

## Table 1
### Patient Procedure and Imaging Setup Summary (Number of Patients)

| Procedure Ablation | S2000 + 10 Fr AcuNav | S2000 + 8 Fr AcuNav | SC2000 + 10 Fr SoundStar | Total |
|---|---|---|---|---|
| Typical AFL | - | - | 2 | 2 |
| Atypical AFL | - | 1 | - | 1 |
| Paroxysmal AF | | 3 | 2 | 5 |
| Persistent AF | 1 | 2 | - | 3 |
| Total | 1 | 6 | 4 | 11 |

AF = atrial fibrillation; AFL = atrial flutter.